blood®
Regular Article

HEMATOPOIESIS AND STEM CELLS

Hif-1α and Hif-2α regulate hemogenic endothelium and hematopoietic stem cell formation in zebrafish

Claudia Gerri,* Michele Marass,* Andrea Rossi, and Didier Y. R. Stainier

Department of Developmental Genetics, Max Planck Institute for Heart and Lung Research, Bad Nauheim, Germany

KEY POINTS

- Hypoxia regulates EHT through Hif-1α and Hif-2α.
- The Hif pathway functions upstream of Notch signaling in HSC formation.

During development, hematopoietic stem cells (HSCs) derive from specialized endothelial cells (ECs) called hemogenic endothelium (HE) via a process called endothelial-to-hematopoietic transition (EHT). Hypoxia-inducible factor-1α (HIF-1α) has been reported to positively modulate EHT in vivo, but current data indicate the existence of other regulators of this process. Here we show that in zebrafish, Hif-2α also positively modulates HSC formation. Specifically, HSC marker gene expression is strongly decreased in *hif-1aa; hif-1ab* (*hif-1α*) and in *hif-2aa;hif-2ab* (*hif-2α*) zebrafish mutants and morphants. Moreover, live imaging studies reveal a positive role for *hif-1α* and *hif-2α* in regulating HE specification. Knockdown of *hif-2α* in *hif-1α* mutants leads to a greater decrease in HSC formation, indicating that *hif-1α* and *hif-2α* have partially overlapping roles in EHT. Furthermore, hypoxic conditions, which strongly stimulate HSC formation in wild-type animals, have little effect in the combined absence of Hif-1α and Hif-2α function. In addition, we present evidence for Hif and Notch working in the same pathway upstream of EHT. Both *notch1a* and *notch1b* mutants display impaired EHT, which cannot be rescued by hypoxia. However, overexpression of the Notch intracellular domain in ECs is sufficient to rescue the *hif-1α* and *hif-2α* morphant EHT phenotype, suggesting that Notch signaling functions downstream of the Hif pathway during HSC formation. Altogether, our data provide genetic evidence that both Hif-1α and Hif-2α regulate EHT upstream of Notch signaling. (*Blood*. 2018;131(9):963-973)

Introduction

Hematopoiesis is the process of blood cell production, and it occurs in 2 waves known as primitive and definitive.[1] In vertebrate embryos, the definitive wave occurs in several locations, including the ventral wall of the dorsal aorta (VDA),[2,3] where a specific subset of endothelial cells (ECs), referred to as hemogenic endothelium (HE), resides. The HE undergoes a process called endothelial-to-hematopoietic transition (EHT) to give rise to hematopoietic stem cells (HSCs). In this process, some ECs acquire hematopoietic potential and subsequently extrude from the VDA to form HSCs.[4-6]

The transcription factor RUNX1 is one of the main players that positively regulates EHT.[6,7] In mice, *Runx1* is required for the formation of intra-arterial clusters and consequently of HSCs.[8] Accordingly, in zebrafish, both knockdown[9,10] and knockout[11] of *runx1* abrogate definitive hematopoiesis from the VDA. A well-known regulator of *Runx1* expression is the Notch signaling pathway. In both mice[12] and zebrafish,[13] loss-of-function models for *Notch1* exhibit a pronounced reduction in *Runx1* expression and consequently impaired definitive hematopoiesis. Mice that lack *Gata2*, a zinc-finger transcription factor gene directly regulated by NOTCH1,[14] show dramatic defects in EHT.[15] The Notch1-Gata2-Runx1 axis is conserved in zebrafish, because Notch1a and Notch1b have been shown to regulate *gata2b* expression,[13] which in turn positively modulates *runx1* transcription in a cell-autonomous manner.[16,17] Downstream of RUNX1 in the EHT molecular cascade lies *cMyb*.[18] Loss-of-function murine[19-21] and fish[22] models for *cMyb* exhibit defects in several steps of hematopoiesis, including HSC differentiation and maintenance.

In recent years, the hypoxia-inducible factor (Hif) pathway has been suggested to be involved in EHT. In zebrafish, experiments that use morpholinos (MOs) against *hif-1ab* and treat the embryos with chemicals such as dimethyloxalylglycine (DMOG) to stabilize Hif-α proteins have led to the suggestion that the Hif pathway is a positive regulator of *runx1* and *cmyb* expression.[23] These data were later supported by studies in mice in which a conditional knockout of *Hif-1α* in vascular endothelial cadherin-expressing cells caused a significant but not complete reduction in HSC numbers, suggesting that other players are involved.[24]

In this study, we generated zebrafish mutants for *hif-2α* (*hif-2aa;hif-2ab*), which exhibit a reduction in ECs undergoing EHT, and show that *hif-1α* and *hif-2α* both play a role in this process. Exposure to hypoxia strongly induces EHT in wild-type (WT) embryos and partially rescues the phenotype in *hif-1α* and *hif-2α* single mutants. In addition, we provide evidence for the hypoxia-Hif pathway acting upstream of Notch signaling in EHT. Altogether, our data provide new insights into the role of the Hif pathway in HSC formation and refine the hierarchy of the EHT transcription cascade.

Methods

Zebrafish handling

Zebrafish were maintained and embryos were obtained and raised under standard conditions[25] in accordance with institutional (Max-Planck-Gesellschaft) and national ethical and animal welfare guidelines.

Tg(kdrl:Hsa.HRAS-mCherry)^{s896},[26] *Tg(kdrl:EGFP)*^{s843},[27] *Tg(cmyb:EGFP)*^{zf169},[28] *Tg(-1.5hsp70l:GAL4)*^{kca4},[29] *(5xUAS-E1b:6xMYC-notch1a)*^{kca3},[30] and *Tg(fli1a:GAL4FF)*^{ubs4},[31] fish were used in this study.

Generation of *hif-2aa*^{bns231} and *hif-2ab*^{bns232} mutants

pT7-gRNA and pT3TS-nlsCas9nls vectors were purchased from Addgene.[32] A guide RNA (gRNA) was designed to target exon 8 of *hif-2aa* using the CRISPR design tool (http://crispr.mit.edu/). Generation of gRNA and Cas9 messenger RNA (mRNA) was performed as described previously.[33] A transcription activator-like effector nuclease (TALEN) targeting exon 3 of *hif-2ab* was designed and cloned using Golden Gate assembly into the pCS2TAL3RR or pCS2TAL3DD expression vectors.[34] Generation of TALEN arm mRNAs was performed as described previously.[33] Mutant alleles were identified by sequencing polymerase chain reaction (PCR) products; bands of 281 and 256 bp for *hif2-aa* and *hif2-ab*, respectively, were purified from a 1% agarose gel and sequenced. gRNA sequences, TALEN repeat of variable diresidues, and primers used for genotyping are listed in supplemental Tables 1, 2, and 3, respectively (available on the *Blood* Web site).

Generation of *notch1a*^{bns135} mutant and genotyping of *notch1b*^{sa11236} mutant

A TALEN targeting exon 11 of *notch1a* was designed and cloned by using Golden Gate assembly into the pCS2TAL3RRR or pCS2TAL3DDD expression vectors.[34] Mutant alleles were identified by high resolution melt analysis[35] of PCR products. *notch1b* mutants were ordered from the European Zebrafish Resource Center. Heterozygous fish were distinguished from WT and homozygous mutant fish by high resolution melt analysis[35] of PCR products. Homozygous mutant and WT fish display a similar melting profile, so to distinguish them, a PCR product of 518 bp was purified from 1% agarose gel and was sent for sequencing. TALEN repeat of variable diresidues and primers for genotyping are listed in supplemental Tables 2 and 3, respectively.

Hypoxia chamber treatment

The hypoxia chamber was flushed with nitrogen gas to reach 3% O_2 concentration (C-Chamber, ProOX 110, ProCO2 from Biospherix) at 28°C. 50-mm Petri dishes containing 4 mL of embryo water were pre-equilibrated in the chamber overnight. Treatments started at 28 hours post fertilization (hpf) for 8 hours.

Imaging

Images and videos were acquired by using an LSM800 confocal laser scanning microscope (Zeiss) or high-end stereoscopic microscopes (Nikon SMZ25) after embryos were anesthetized with a low dose of tricaine and immobilized in 1% low-melting agarose in glass-bottom Petri dishes (MatTek Corporation, Ashland, MA). Time-lapse images were recorded every 15 minutes for a maximum period of ~14 hours. The microscope stage was enclosed in a temperature-controlled chamber at 28°C.

Quantitative PCR

Quantitative PCR (qPCR) was performed on complementary DNA obtained from whole embryo or isolated trunk RNA extracted by using TRIZOL (Life Technologies).[36] For isolation of embryo trunks, a pool of 36 hpf embryos (~100 per tube) was subjected to pipetting through a 200-μL pipette for 90 seconds. After centrifugation at 100*g* for 3 minutes, the solution was transferred into a dish containing cold Hank's salt solution to select and collect only the trunks under a dissecting microscope. Complementary DNA was synthesized by using SuperScript III RT (Invitrogen) with 300 μg of RNA. A Bio-Rad Real-Time PCR System was used for qPCR experiments. All reactions were performed in 3 technical replicates, and the results represent 3 independent biological samples. qPCR primers are listed in supplemental Table 4.

Whole-mount in situ hybridization

Whole-mount in situ hybridization (WISH) was performed as described previously.[37] Primers used to make WISH probes are listed in supplemental Table 5. If genotyping was necessary after imaging, the embryos were placed individually into PCR tubes with 10 μL of 50 mM NaOH. The samples were incubated at 95°C for 20 to 30 minutes (vortexing), and then 1 μL of 1 M tris (hydroxymethyl)aminomethane [pH 8.0] was added to the solution. The extracted DNA was used for genotyping.

MO injections

MOs targeting *hif-1aa*,[38] *hif-1ab*,[39] *hif-2aa*,[38] *hif-2ab*,[38] and the control standard MO were purchased from Gene Tools (Eugene, OR). After optimal titration (no overt toxic effects were observed), *hif-1aa* and *hif-1ab* MOs were injected at the 1-cell stage at 0.5 ng per embryo, and *hif-2aa* and *hif-2ab* MOs were injected at 1 ng per embryo. MO sequences are listed in supplemental Table 6.

Overexpression of Notch intracellular domain

Progeny from *Tg(-1.5hsp70l:GAL4)*^{kca4};*(5xUAS-E1b:6xMYC-notch1a)*^{kca3} fish as well as WT embryos were subjected to 37°C heat shock at 14 or 20 hpf for 50 minutes. The embryos were then kept at 28°C until 36 hpf, when they were fixed and processed for WISH. *Tg(fli1a:GAL4FF)*^{ubs4} were mated to *(5xUAS-E1b:6xMYC-notch1a)*^{kca3}, and the resulting embryos were processed for WISH at 36 hpf. The embryos were selected according to their phenotype and were photographed and subsequently genotyped for *Tg(fli1a:GAL4FF)*^{ubs4} and *Tg(5xUAS-E1b:6xMYC-notch1a)*^{kca3}. Primers used for genotyping are listed in supplemental Table 3.

Overexpression of *vegfaa* and *evi1*

Full-length $vegfaa_{121}$ and *evi1* coding sequences were cloned into pCS2^{+}. mRNAs were synthesized by using an mMESSAGE mMACHINE SP6 in vitro transcription kit. Zebrafish embryos were injected at the 1-cell stage with 50 pg of *vegfaa* mRNA or 250 pg of *evi1* mRNA.

Quantification and statistical analysis

For the quantification shown in Figure 2D, we counted the number of cells co-expressing *Tg*(*cmyb*:EGFP) and *Tg*(*kdrl*:mCherry) within as well as emerging from the VDA at 36 hpf in a 10-somite-long trunk area above the yolk extension. *hif-1aa*$^{+/-}$;*hif-1ab*$^{+/-}$ fish were identified by genotyping and incrossed, and the resulting embryos were processed for the WISH experiments shown in Figures 1 and 4. The same procedure was followed for *hif-2aa*$^{+/-}$;*hif-2ab*$^{+/-}$, and results are shown in Figures 1 and 4. For the experiments shown in Figure 5 and supplemental Figure 14, *notch1a*$^{+/-}$ fish

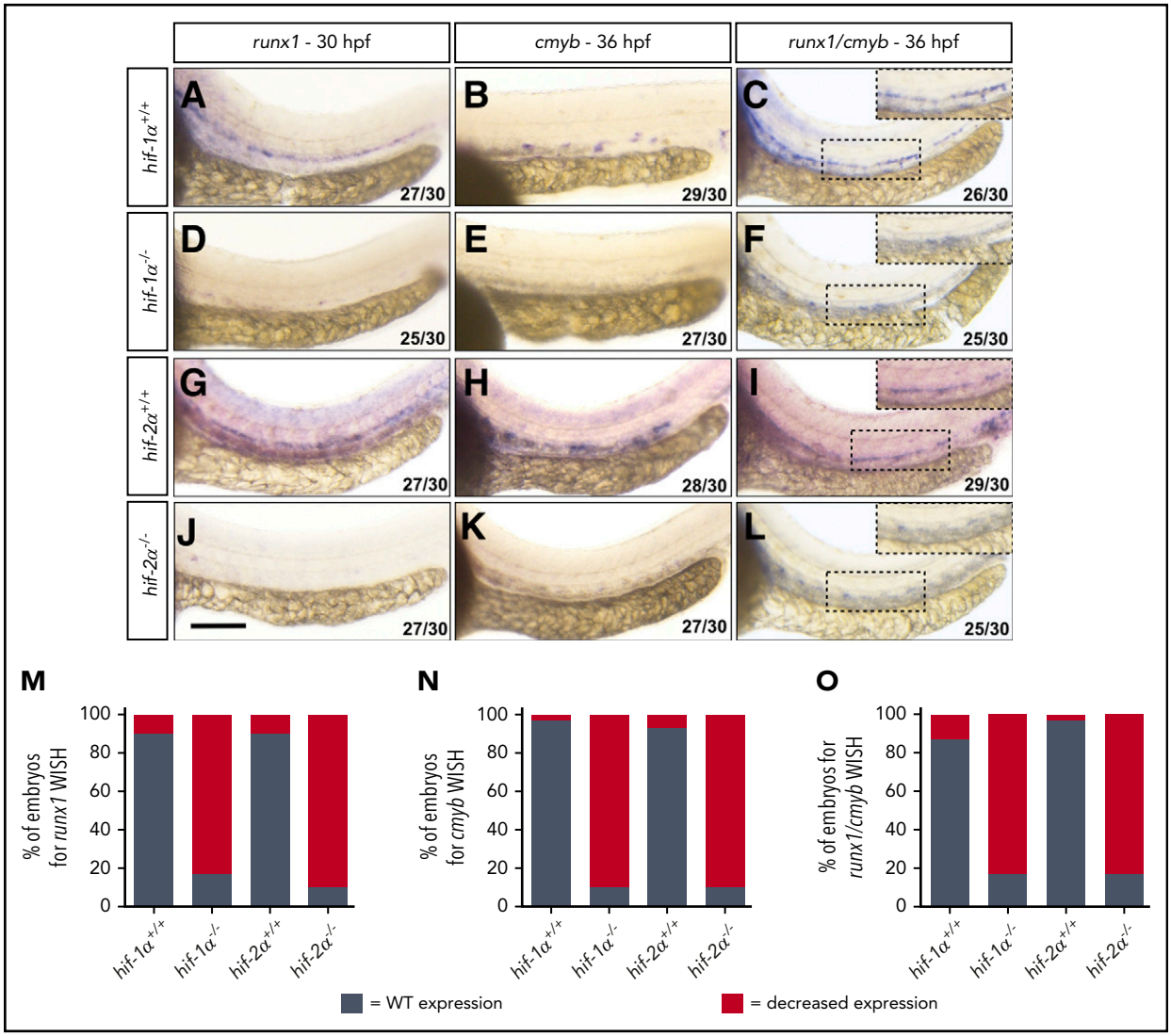

Figure 1. *hif-1α*$^{-/-}$ and *hif-2α*$^{-/-}$ exhibit decreased *runx1* and *cmyb* expression. (A-L) Brightfield images of WISH for *runx1*, *cmyb*, and *runx1/cmyb* expression in (A-C and G-I) WT sibling, (D-F) *hif-1α*$^{-/-}$, and (J-L) *hif-2α*$^{-/-}$ embryos (stages shown in the figure). The VDA region is outlined and shown at higher magnification in C, F, I, and L (lateral views). Scale bar, 100 μm. (M-O) Quantification of *runx1* (A, D, G, and J), *cmyb* (B, E, H, and K), and *runx1/cmyb* (C, F, I, and L) WISH results, showing the percentages of embryos with WT and decreased expression in the genotypes listed. n/n, number of embryos showing representative phenotype/total number of embryos examined.

were incrossed, and the resulting progeny were processed for WISH. Next, the embryos were selected on the basis of their phenotype, photographed, and processed for genotyping as described above. The same procedure was followed for *notch1b*$^{+/-}$ fish; results are shown in Figure 5 and supplemental Figure 14. The quantification of phenotypes observed by WISH is represented in the figures as n/n (number of embryos showing representative phenotype/total number of embryos examined). Statistical analysis was performed by using GraphPad software. Data in bar graphs represent mean with standard error of the mean or standard deviation. *P* values were calculated by Student *t* test for single comparisons of normally distributed data.

Results

hif-1α and *hif-2α* mutations lead to a reduced number of HE cells undergoing EHT

To investigate the role of the Hif pathway in EHT, we analyzed *hif-1aa*^{bns89};*hif-1ab*^{bns90} and *hif-2aa*^{bns231};*hif-2ab*^{bns232} double mutants,[33] hereafter abbreviated as *hif-1α* mutants (*hif-1α*$^{-/-}$), and *hif-2α* mutants (*hif-2α*$^{-/-}$), respectively. *hif-2aa* mutants were generated by using the CRISPR/Cas9 technology[40] to target a region in exon 8 that encodes the second PAS domain (supplemental Figure 1A). *hif-2ab* mutants were generated by using TALEN technology[34] to target a region in exon 3 that encodes the first PAS domain (supplemental Figure 2A). We recovered 2 alleles, *hif-2aa*^{bns231} and *hif-2ab*^{bns232}, carrying out-of-frame mutations that led to a premature stop codon after 26 missense amino acids or 1 missense amino acid, respectively (supplemental Figures 1B-C and 2B-C). To investigate the severity of the mutant alleles, we analyzed *hif-2aa* and *hif-2ab* mRNA levels by qPCR. When compared with WT siblings, *hif-2aa*^{bns231} and *hif-2ab*^{bns232} mutants display a reduction in the mRNA levels of ~30% in the mutated gene (supplemental Figures 1D and 2D). To determine whether these mutants exhibit defects in HSC formation, we performed WISH for *runx1*, one of the earliest known markers of HSC fate. Compared with their WT siblings (Figure 1A,G,M), both *hif-1α*$^{-/-}$ and *hif-2α*$^{-/-}$ display a reduction in *runx1* expression in

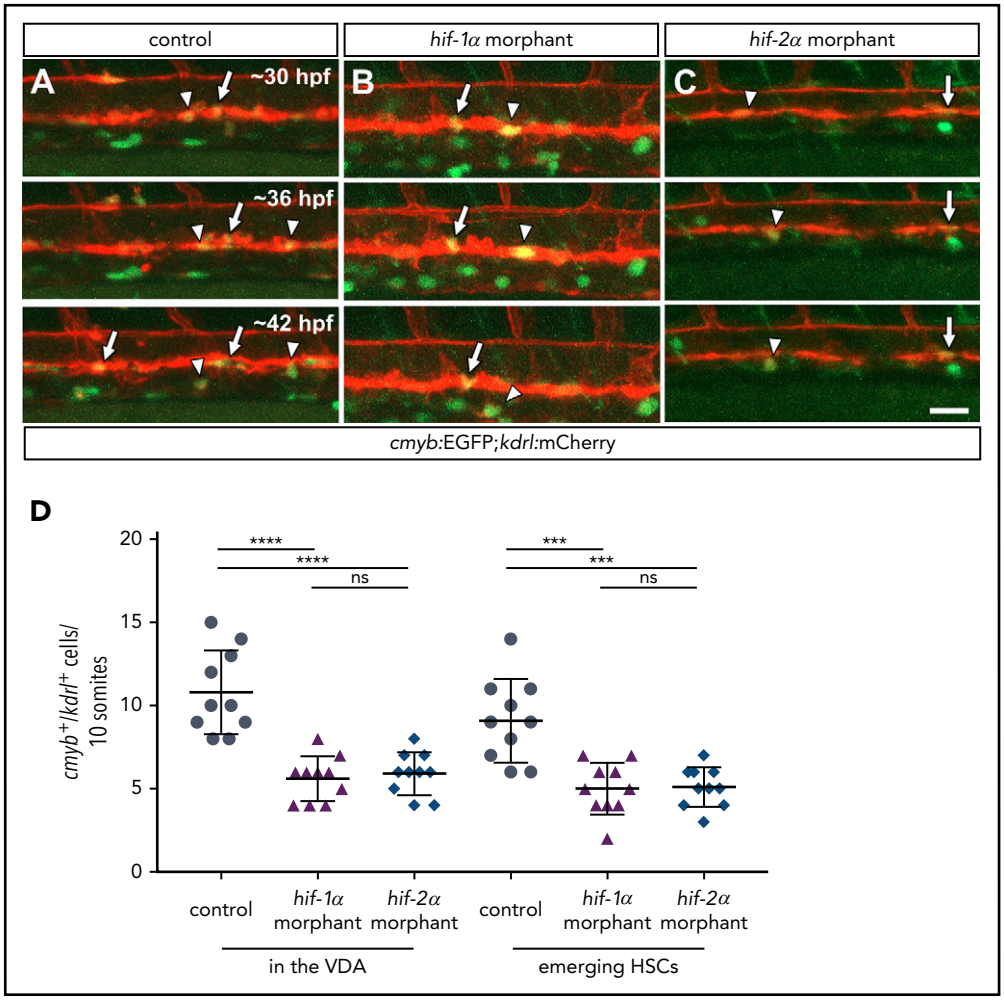

Figure 2. *hif-1α* and *hif-2α* morphants show reduced numbers of *cmyb*:EGFP$^+$;*kdrl*:mCherry$^+$ cells in the VDA. (A-C) Maximal intensity projections of time-lapse confocal images of 36 hpf *Tg(cmyb:EGFP);Tg(kdrl:mCherry)* control and *hif-1α* and *hif-2α* morphants. Arrows point to *cmyb*:EGFP$^+$;*kdrl*:mCherry$^+$ cells in the VDA, and arrowheads point to *cmyb*:EGFP$^+$;*kdrl*:mCherry$^+$ emerging HSCs. Scale bar, 50 μm. (D) Quantification of *cmyb*:EGFP$^+$;*kdrl*:mCherry$^+$ cells in the VDA and emerging HSCs in a 10-somite-long trunk area in control and *hif-1α* and *hif-2α* morphants (lateral views) (n = 10 embryos from 3 different clutches). ***$P < .001$; ****$P < .0001$. ns, not significant (Student *t* test).

the VDA at 30 hpf (Figure 1D,J,M). In addition, we analyzed at 36 hpf the expression levels of *cmyb*, an important transcription factor gene downstream of Runx1 in the EHT cascade.[41] In WT siblings, *cmyb* was expressed in cells located in both the VDA and caudal hematopoietic tissue (Figure 1B,H,N; supplemental Figure 3A,C,E), and *cmyb*$^+$ cell numbers were strongly reduced in both *hif-1α*$^{-/-}$ and *hif-2α*$^{-/-}$ (Figure 1E,K,N; supplemental Figure 3B,D,E). Consistent with these results, *hif-1α*$^{-/-}$ and *hif-2α*$^{-/-}$ embryos (Figure 1F,L,O) exhibited a striking decrease in *runx1/cmyb* expression levels at 36 hpf compared with WT siblings (Figure 1C,I,O). Similarly, embryos co-injected with *hif-1aa* and *hif-1ab* or *hif-2aa* and *hif-2ab* MOs (hereafter referred to as *hif-1α* morphants and *hif-2α* morphants, respectively) exhibited a decrease in *runx1* and *cmyb* expression levels compared with control MO-injected embryos (supplemental Figure 4). In addition, to test whether the development of the dorsal aorta (DA) was affected in the mutants, we performed WISH for *efnb2a* (an arterial marker) at 36 hpf. *hif-1α*$^{-/-}$ and *hif-2α*$^{-/-}$ exhibited an *efnb2a* expression level similar to that of their WT siblings (supplemental Figure 5). To further investigate the development of the DA, we analyzed axial vessel formation by confocal imaging using the *Tg(kdrl:EGFP)*^{s843} reporter line. We did not observe vascular anomalies in mutant compared with WT embryos (supplemental Figure 6A-C), suggesting that the EHT phenotype observed in *hif-1α*$^{-/-}$ and *hif-2α*$^{-/-}$ is not a result of defects in vascular development.

runx1 is also expressed in blood precursors during primitive hematopoiesis.[9] To test whether primitive hematopoiesis was affected in *hif-1α*$^{-/-}$ and *hif-2α*$^{-/-}$, we analyzed the expression levels of the lateral plate mesoderm markers *runx1* and *gata1a* several hours before the heart starts beating. We detected WT expression levels of these markers in the lateral plate mesoderm of *hif-1α*$^{-/-}$ and *hif-2α*$^{-/-}$ (supplemental Figure 7), indicating that the Hif pathway regulates *runx1* expression only during definitive hematopoiesis. To assess whether erythrocyte number or blood flow was affected, we performed WISH for *gata1a* at 36 hpf as well as brightfield microscopy on live embryos, and we observed WT-like blood development and flow in *hif-1α*$^{-/-}$ and *hif-2α*$^{-/-}$ (supplemental Figure 8 and supplemental Videos 1-3).

HSC formation requires 2 sequential steps: HE specification and the emergence of HSCs from this specialized endothelium via

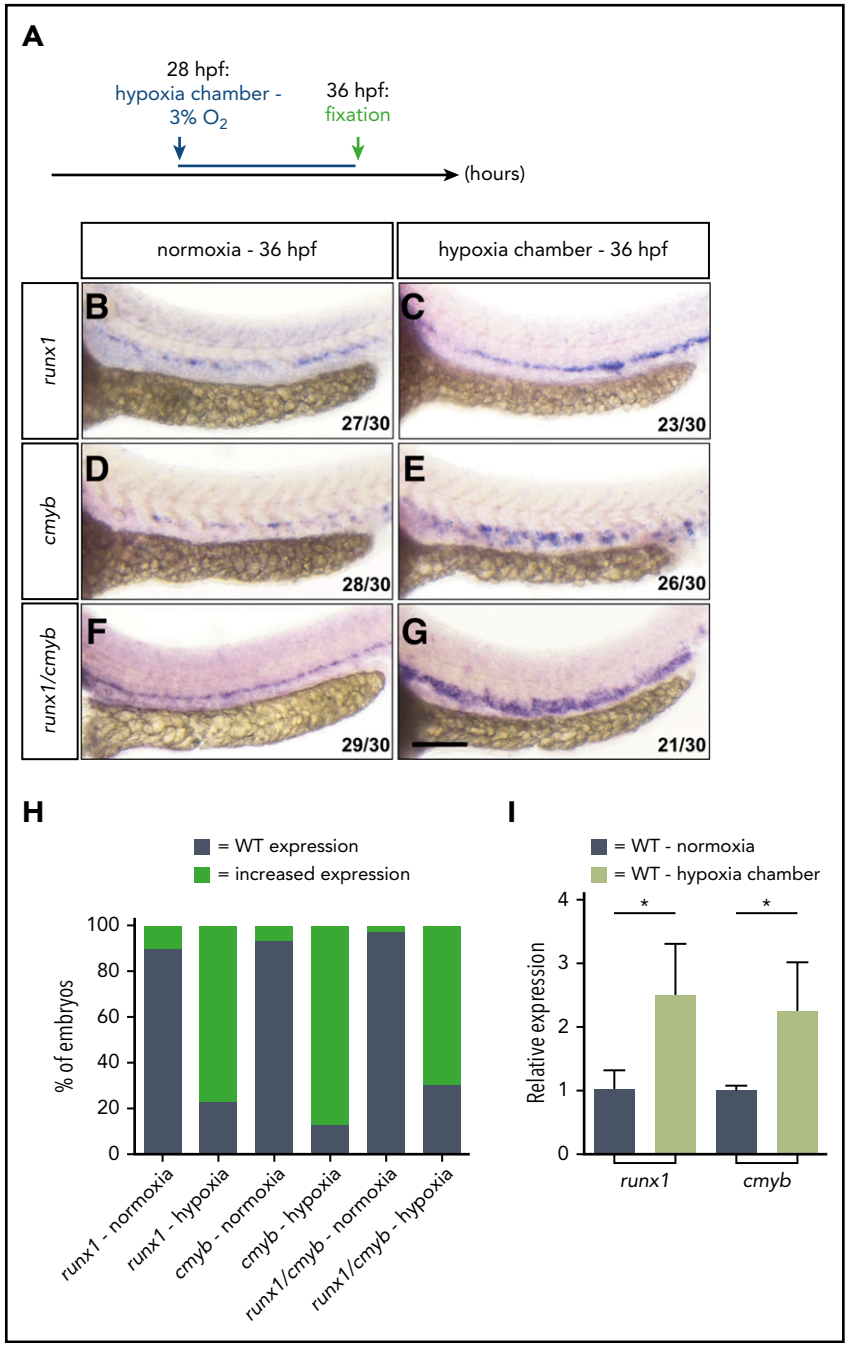

Figure 3. Hypoxia is a potent inducer of HSC formation. (A) Schematic representation of the experiment shown in B-H. (B-G) Brightfield images of WISH for (B-C) *runx1*, (D-E) *cmyb*, and (F-G) *runx1/cmyb* expression in 36 hpf WT embryos in normoxia and after hypoxia exposure for 8 hours starting at 28 hpf (lateral views). Scale bar, 100 μm. (H) Quantification of *runx1* (B-C), *cmyb* (D-E), and *runx1/cmyb* (F-G) WISH results, showing the percentages of embryos with WT and increased expression in each condition. (I) qPCR analysis of *runx1* and *cmyb* mRNA levels in 36 hpf WT embryos in normoxia and after hypoxia exposure for 8 hours starting at 28 hpf (data for whole embryos is shown; data for dissected trunk is provided in supplemental Figure 11). Values represent mean plus SD (n = 3 biological replicates). Ct values for each gene in WT samples in normoxia: *rpl13* = 17.25; *runx1* = 28.23; *cmyb* = 24.48. **P* < .05 (Student *t* test).

EHT.[5] To gain further insights into the precise role of *hif-1α* and *hif-2α* in this process, we performed time-lapse live imaging on *Tg(cmyb:EGFP)*^{zf169}*;Tg(kdrl:Hsa.HRAS-mCherry)*^{s896} embryos, hereafter *Tg(cmyb:EGFP);(kdrl:mCherry)*, injected with control or *hif-1α* or *hif-2α* MOs. By using this transgenic background, it is possible to visualize the HE as cells co-expressing *cmyb*:EGFP;*kdrl*:mCherry in the VDA.[6] Notably, we observed that *hif-1α* and *hif-2α* morphants exhibit a reduced number of *cmyb*:EGFP;*kdrl*:mCherry double-positive cells in the VDA compared with control MO-injected embryos (Figure 2A-C; supplemental Videos 4-6), as confirmed by quantification (Figure 2D). Altogether, these observations suggest that Hif-1α and Hif-2α positively regulate *runx1* and *cmyb* expression, thus modulating HE specification, and consequently resulting in a decreased number of emerging HSCs.

Hypoxia strongly induces HSC formation

Mimicking hypoxia with chemicals like DMOG (a pan-hydroxylase inhibitor) reportedly promotes HSC formation in zebrafish.[23] To better investigate the impact of hypoxia on EHT, WT embryos were exposed to hypoxia for 8 hours using a hypoxia chamber set at 3% O_2, and *runx1* and *cmyb* expression levels were subsequently analyzed by WISH (Figure 3A). WT embryos exposed to hypoxia displayed a strong increase in *runx1* and *cmyb* expression in the VDA at 36 hpf compared with siblings kept in normoxia (Figure 3B-H). To test whether hypoxia exposure affects DA development, we analyzed *efnb2a* expression by WISH and observed similar expression levels between animals kept in normoxia and those exposed to hypoxia (supplemental Figure 9A-B,E). These data were further confirmed by confocal imaging of

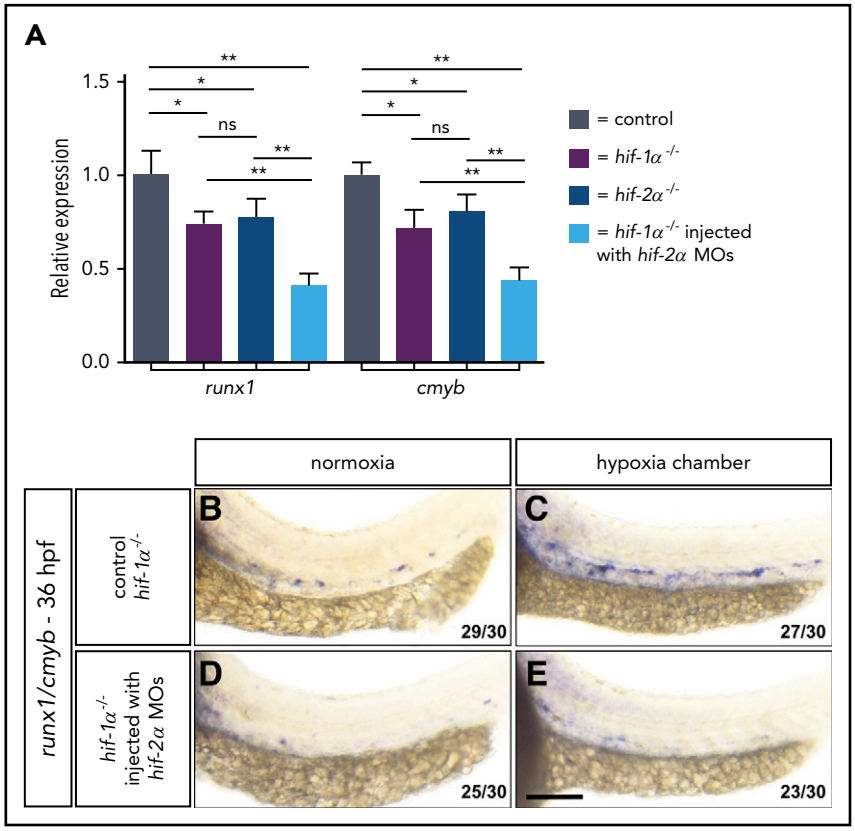

Figure 4. Both *hif-1α* and *hif-2α* function in EHT. (A) qPCR analysis of *runx1* and *cmyb* mRNA levels in 36 hpf controls, *hif-1α*$^{-/-}$, *hif-2α*$^{-/-}$, and *hif-2α* MO-injected *hif-1α*$^{-/-}$. Values represent mean plus standard deviation (SD) (n = 3 biological replicates). Ct values for each gene in WT samples: *rpl13* = 18.11; *runx1* = 27.87; *cmyb* = 25.81. (B-E) Brightfield images of WISH for *runx1/cmyb* expression in 36 hpf (B-C) control MO-injected *hif-1α*$^{-/-}$ and (D-E) *hif-2α* MO-injected *hif-1α*$^{-/-}$ in normoxia and after hypoxia exposure for 8 hours starting at 28 hpf (lateral views). Scale bar, 100 μm. *$P < .05$; **$P < .01$ (Student *t* test).

vascular development using the *Tg(kdrl:EGFP)* line (supplemental Figure 6C-D). Moreover, after performing WISH for *gata1a* at 36 hpf, we did not detect obvious variations in erythrocyte formation after hypoxia exposure (supplemental Figure 10A-B,E), which suggests that the increase in *runx1/cmyb* expression observed is not a result of an increased number of erythrocytes. To further investigate this phenotype, we performed transcriptional analysis on both whole embryos and isolated trunks at 36 hpf in normoxia and after hypoxia. Our qPCR data show that *runx1* and *cmyb* mRNA levels were significantly upregulated in WT animals after hypoxia compared with siblings in normoxia (Figure 3I; supplemental Figure 11A). Taken together, these data suggest that hypoxia is a potent inducer of EHT through strong induction of *runx1* and *cmyb* expression.

Both *hif-1α* and *hif-2α* function in EHT

HIF-2α has been described to have both distinct and overlapping roles with HIF-1α, depending on the biological context.[42] *hif-1α*$^{-/-}$ and *hif-2α*$^{-/-}$ exhibit similar EHT phenotypes (Figure 1), suggesting a shared function for *hif-1α* and *hif-2α* in HE specification in zebrafish. To test this hypothesis, we analyzed *runx1* and *cmyb* mRNA levels in *hif-1α*$^{-/-}$ and *hif-2α*$^{-/-}$ by qPCR on 36 hpf whole embryos and isolated trunks and found that they were reduced by ~30% in both *hif-1α*$^{-/-}$ and *hif-2α*$^{-/-}$ compared with WT sibling embryos (Figure 4A; supplemental Figure 11B). Next, we performed *hif-2α* MO knockdown in *hif-1α*$^{-/-}$ and assessed *runx1* and *cmyb* mRNA levels at 36 hpf. *hif-2α* MO-injected *hif-1α*$^{-/-}$ exhibited a decrease in *runx1* and *cmyb* expression of ~60% compared with control MO-injected embryos and of ~50% compared with *hif-1α*$^{-/-}$ (Figure 4A). These results suggest that *hif-1α* and *hif-2α* have similar roles in EHT.

To further investigate this hypothesis, we exposed control MO-injected *hif-1α*$^{-/-}$ embryos to hypoxic conditions and examined *runx1/cmyb* expression by WISH. Interestingly, after hypoxia exposure, *runx1/cmyb* expression levels were increased compared with normoxia (Figure 4B-C), but this expression was not comparable to the strong *runx1/cmyb* induction observed in WT animals after hypoxia (Figure 3G). This result suggests that hypoxia can rescue, at least in part, the EHT phenotype observed in *hif-1α*$^{-/-}$, possibly through *hif-2α*. To test this hypothesis, we analyzed *runx1/cmyb* expression levels in *hif-2α* MO-injected *hif-1α*$^{-/-}$ in both normoxic and hypoxic conditions. In normoxia, these embryos showed a further decrease in *runx1/cmyb* expression (Figure 4D) compared with control MO-injected *hif-1α*$^{-/-}$ (Figure 4B). Importantly, when *hif-2α* MO-injected *hif-1α*$^{-/-}$ embryos were exposed to hypoxia, the rescue in *runx1/cmyb* expression was completely abrogated (Figure 4C,E). These observations show that hypoxia, signaling through Hif-2α, can partially rescue the EHT phenotype observed in *hif-1α*$^{-/-}$.

Hypoxia does not rescue the EHT defects in *notch1a* or *notch1b* mutants

It has been shown that Notch signaling is a key regulator of EHT. Notch1a and Notch1b modulate *gata2b* expression, and Gata2b in turn directly regulates *runx1* transcription.[12-15,43] First, we analyzed whether *notch1a*, *notch1b*, and *gata2b* mRNA levels were influenced by changes in O_2 concentration and found that they were strongly induced after hypoxic conditions compared with sibling embryos in normoxic conditions (Figure 5A; supplemental Figure 12). We also tested whether *notch1a*, *notch1b*, and *gata2b* mRNA levels were altered in the absence of *hif-1α*

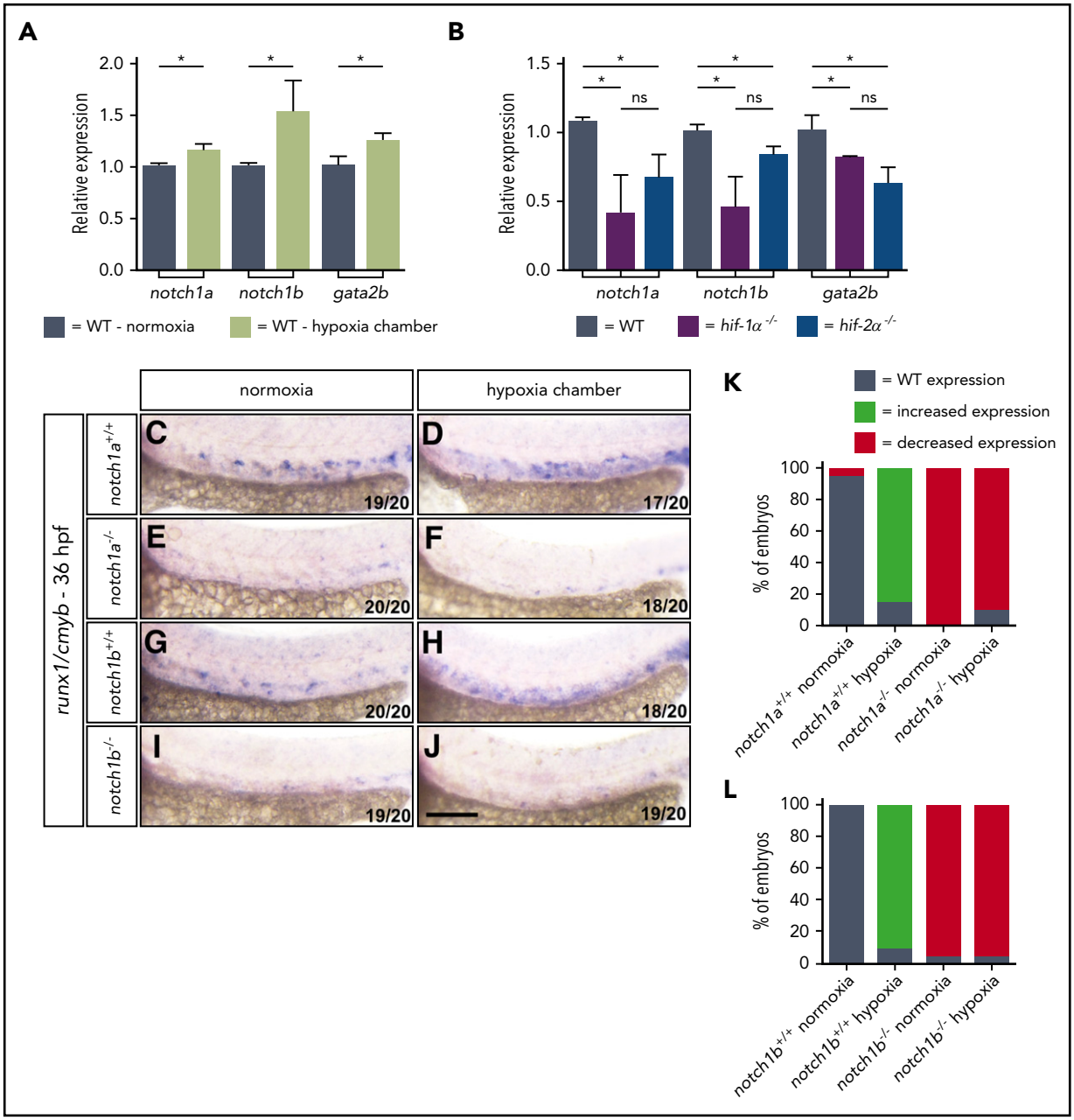

Figure 5. Hypoxia does not rescue the EHT defects in *notch1a* or *notch1b* mutants. (A) qPCR analysis of *notch1a*, *notch1b*, and *gata2b* mRNA levels in 36 hpf WT embryos in normoxia and after hypoxia exposure for 8 hours starting at 28 hpf. (B) qPCR analysis of *notch1a*, *notch1b*, and *gata2b* mRNA levels in 36 hpf WT, *hif-1α*$^{-/-}$ and *hif-2α*$^{-/-}$ embryos. Values represent mean plus SD (n = 3 biological replicates). Ct values for each gene in WT samples: *rpl13* = 17.05; *notch1a* = 21.22; *notch1b* = 22.21; *gata2b* = 28.33. (C-J) Brightfield images of WISH for *runx1/cmyb* expression in 36 hpf (C-D, and G-H) WT siblings, (E-F) *notch1a*$^{-/-}$, and (I-J) *notch1b*$^{-/-}$ embryos in normoxia and after hypoxia exposure for 8 hours starting at 28 hpf (lateral views). Scale bar, 100 μm. (K) Quantification of *runx1/cmyb* WISH results (C-F), showing the percentages of embryos with WT, increased expression, and decreased expression in each condition. (L) Quantification of *runx1/cmyb* WISH results (G-J), showing the percentages of embryos with WT, increased expression, and decreased expression in each condition. *$P < .05$ (Student *t* test).

and *hif-2α* function. In both *hif-1α*$^{-/-}$ and *hif-2α*$^{-/-}$, we observed a significant reduction in mRNA levels for all 3 genes compared with WT siblings (Figure 5B). These results suggest that Notch acts downstream of the Hif pathway during EHT in zebrafish. To test this hypothesis, we took advantage of *notch1a* and *notch1b* mutant alleles available in our laboratory. *notch1a*$^{-/-}$ was generated by TALEN technology targeting a region in exon 11 that encodes an EGF-like repeat in the extracellular portion of the receptor (supplemental Figure 13A). We recovered an allele, *notch1a*^{bns135}, carrying an out-of-frame mutation that led to a premature stop codon after 19 missense amino acids (supplemental Figure 13B-C). *notch1b*^{sa11236} mutants[44] contain a T→A transversion in exon 21 (supplemental Figure 13D), which led to a premature stop codon in the extracellular part of the protein (supplemental Figure 13E). First, we tested whether *notch1a*$^{-/-}$ and *notch1b*$^{-/-}$ recapitulate the previously published EHT phenotypes using *notch1a* and *notch1b* MOs.[13] When we incrossed *notch1a*$^{+/-}$ or *notch1b*$^{+/-}$, we observed a reduction in *runx1/cmyb* and *gata2b* expression by WISH in both *notch1a*$^{-/-}$ and *notch1b*$^{-/-}$ compared with WT siblings (supplemental Figure 14), as reported in *notch1a* and *notch1b* morphants.[13] We then used these mutants to investigate the molecular hierarchy

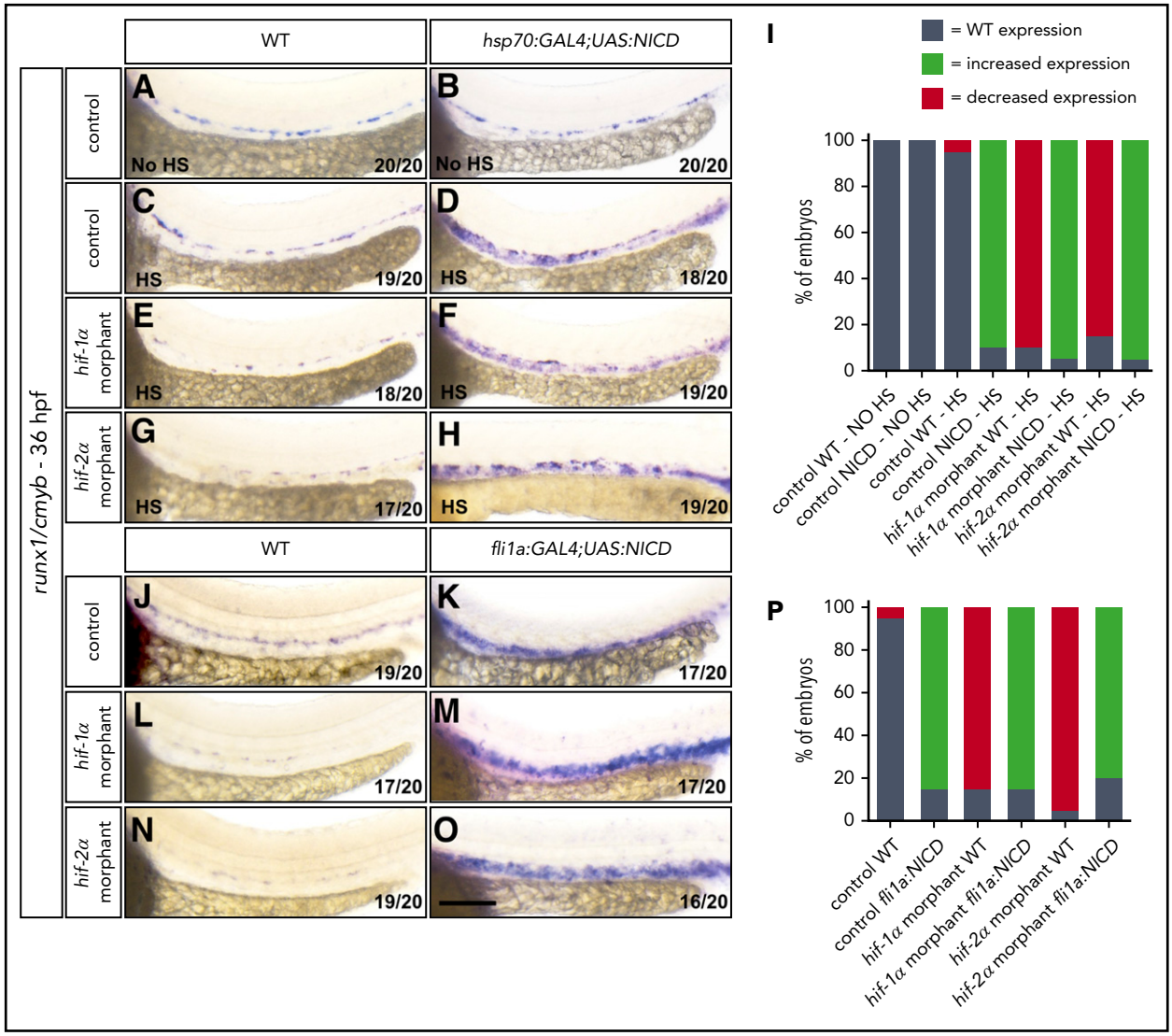

Figure 6. NICD overexpression in ECs rescues the EHT defects in *hif-1α* and *hif-2α* morphants. (A-H) Brightfield images of WISH for *runx1/cmyb* expression in (A-B) 36 hpf control MO-injected WT and *Tg(hsp70:GAL4;UAS:NICD)* embryos at 28°C, (C-D) control MO-injected WT and *Tg(hsp70:GAL4;UAS:NICD)* embryos after heat shock, (E-F) *hif-1α* MO-injected WT and *Tg(hsp70:GAL4;UAS:NICD)* embryos after heat shock, and (G-H) *hif-2α* MO-injected WT and *Tg(hsp70:GAL4;UAS:NICD)* embryos after heat shock. (I) Quantification of *runx1/cmyb* WISH results (A-H), showing the percentages of embryos with WT, increased expression, and decreased expression in each condition. (J-O) Brightfield images of WISH for *runx1/cmyb* expression in (J-K) 36 hpf control MO-injected WT and *Tg(fli1a:GAL4;UAS:NICD)* embryos, (L-M) *hif-1α* MO-injected WT and *Tg(fli1a:GAL4;UAS:NICD)* embryos, and (N-O) *hif-2α* MO-injected WT and *Tg(fli1a:GAL4;UAS:NICD)* embryos (lateral views). (P) Quantification of *runx1/cmyb* WISH results (J-O), showing the percentages of embryos with WT, increased expression, and decreased expression in each condition. Scale bar, 100 μm.

between Hif and Notch signaling during EHT. We exposed embryos from *notch1a*$^{+/-}$ or *notch1b*$^{+/-}$ incrosses to normoxia or hypoxia and analyzed *runx1/cmyb* expression levels by WISH. WT sibling embryos exposed to hypoxia exhibited an increase in *runx1/cmyb* expression (Figure 5C-D,G-H,K-L) but *notch1a*$^{-/-}$ or *notch1b*$^{-/-}$ embryos did not (Figure 5E-F,I-L). These data show that hypoxia does not induce *runx1* or *cmyb* expression in *notch1a*$^{-/-}$ or *notch1b*$^{-/-}$, unlike what is observed in WT embryos, and thus does not rescue their EHT phenotype. Altogether, our results suggest that Hif and Notch function in the same pathway during EHT.

Activation of Notch signaling in ECs can rescue *hif-1α* and *hif-2α* EHT defects

To further investigate the hierarchy between Hif and Notch signaling, we overexpressed the *notch1a* intracellular domain (NICD) to promote Notch signaling activation in a temporally controlled manner. We used the *Tg(-1.5hsp70l:GAL4)*^{kca4}*;(5xUAS-E1b:6xMYC-notch1a)*^{kca3} line, hereafter, *Tg(hsp70:GAL4;UAS:NICD)*, to drive NICD overexpression upon heat shock treatment. Specifically, we analyzed control MO-injected WT and *Tg(hsp70:GAL4;UAS:NICD)* animals kept at 28°C and observed that *runx1/cmyb* expression was indistinguishable between these two populations (Figure 6A-B,I). In parallel, control MO-injected WT and *Tg(hsp70:GAL4;UAS:NICD)* embryos were subjected to heat shock at 37°C for 50 minutes at both 14[45] and 20 hpf[46] and were analyzed by WISH for *runx1/cmyb* at 36 hpf. After heat shock, we did not observe changes in *runx1/cmyb* expression in control WT embryos (Figure 6C), but *Tg(hsp70:GAL4;UAS:NICD)* embryos exhibited enhanced expression of HSC markers in the VDA (Figure 6D,I; supplemental Figure 15A-B,G). To assess DA formation, we first examined *efnb2a* expression by WISH and found that it was slightly

increased upon heat shock; however, it was not expressed ectopically compared with *Tg(hsp70:GAL4;UAS:NICD)* embryos left at 28°C (supplemental Figure 9C-E). To investigate the vascular pattern, we analyzed *Tg(kdrl*:EGFP) expression in *Tg (hsp70:GAL4;UAS:NICD)* embryos and did not detect vascular abnormalities after heat shock (supplemental Figure 6E-F). Furthermore, to analyze whether erythrocyte formation was affected, we performed WISH for *gata1a* at 36 hpf and observed no significant changes in *Tg(hsp70:GAL4;UAS:NICD)* embryos after heat shock (supplemental Figure 10C-E). Next, we analyzed *runx1/cmyb* levels in *hif-1α* or *hif-2α* MO-injected WT and *Tg(hsp70:GAL4;UAS:NICD)* embryos. In nontransgenic *hif-1α* and *hif-2α* morphants, we observed a decrease in *runx1/cmyb* expression (supplemental Figure 4), which was not influenced by heat shock treatment (Figure 6E,G,I). Conversely, in *Tg(hsp70:GAL4;UAS:NICD)* embryos injected with *hif-1α* or *hif-2α* MOs, we could detect a strong induction of *runx1/cmyb* expression after heat shock (Figure 6F,H,I; supplemental Figure 15C-G), thereby rescuing the defects observed in *hif-1α* and *hif-2α* morphants. To further investigate this ability of Notch signaling to rescue, we took advantage of the double transgenic line *Tg(fli1a:GAL4FF)*^{ubs4}*;(5xUAS-E1b:6xMYC-notch1a)*^{kca3}, hereafter, *Tg(fli1a:GAL4;UAS:NICD)*, to overexpress NICD specifically in ECs. We observed high expression levels of *runx1/cmyb* in control MO-injected *Tg(fli1a:GAL4;UAS:NICD)* embryos compared with control MO-injected WT siblings (Figure 6J-K,P). Next, we injected *hif-1α* or *hif-2α* MOs into WT and *Tg(fli1a:GAL4;UAS:NICD)* embryos. In nontransgenic *hif-1α* and *hif-2α* morphants, we observed a reduction in *runx1/cmyb* expression (Figure 6L,N,P). Conversely, in *Tg(fli1a:GAL4;UAS:NICD)* embryos injected with *hif-1α* or *hif-2α* MOs, the expression of *runx1/cmyb* was strongly induced, rescuing the *hif-1α* and *hif-2α* morphant phenotypes (Figure 6M,O-P). These data indicate that global as well as endothelial-specific NICD overexpression can rescue the EHT defects observed in Hif-1α and Hif-2α loss-of-function models.

To further characterize the link between Hif and Notch signaling, we tested whether the overexpression of *evi1* or *vegfaa* was able to rescue the EHT phenotype observed in *hif-1α* and *hif-2α* mutants. As previously described,[46] the overexpression of these 2 genes leads to an increase in *notch1b* expression levels in HE during EHT. Interestingly, the injection of *evi1* or *vegfaa* mRNA in *hif-1α*$^{-/-}$ and *hif-2α*$^{-/-}$ rescued *runx1/cmyb* expression (supplemental Figure 16), which suggests that *evi1* and *vegfaa* function downstream or in parallel to the Hif pathway during EHT. Altogether, our observations suggest that Notch signaling functions downstream of hypoxia and the Hif pathway during EHT.

Discussion

The differentiation of cell lineages from pluripotent stem cells has been achieved in vitro by inducing the expression of transcription factors or exposing pluripotent cells to morphogens. Notably, most of the molecules identified to promote cell specification in vitro were reported to play a role during embryonic development. Many groups have been trying to develop HSC-like cells in vitro but have not yet obtained successful long-term engraftments in mouse recipients.[47-52] One recent publication showed advances in the robustness of HSC engraftment into mouse hosts, leaving room for improvement.[53] Another recent article described a method to reprogram adult ECs to HSCs through transient expression of transcription factors and vascular niche-derived

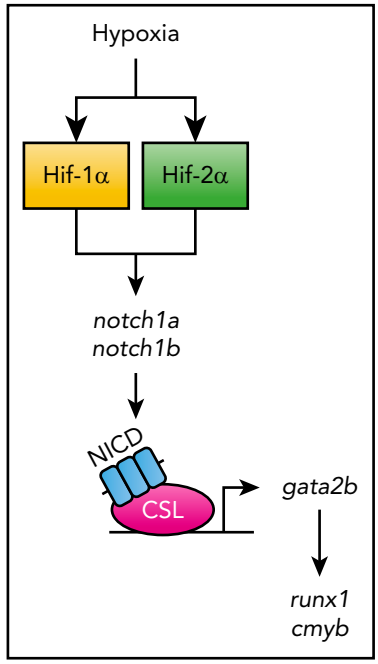

Figure 7. Proposed model. Schematic illustration of the role of the Hif pathway during EHT. We propose that Hif functions upstream of Notch1 signaling in EHT.

angiocrine signals.[54] A better understanding of all the players involved in hematopoiesis and how intrinsic and extrinsic factors are coordinated in the vascular niche could have a significant impact on the generation of therapy-grade HSCs. Here, by using a genetic approach in zebrafish, we describe a novel role for *hif-2α* in HSC formation and confirm previous reports on *hif-1α* in this process. Moreover, we provide evidence for the Hif pathway functioning upstream of Notch signaling during EHT (Figure 7).

In a previous article, Harris et al[23] showed that the stabilization of Hif-α subunits with chemicals such as DMOG can strongly induce *runx1* and *cmyb* expression during EHT. These experiments suggested a role for the Hif pathway in this process but did not explore the role of O_2 concentration and could not exclude possible adverse effects of DMOG.[55] In our study, we exposed zebrafish embryos to hypoxic conditions using a hypoxia chamber at 3% O_2 concentration. Embryos exposed to hypoxia exhibited increased expression of HSC markers in the VDA, suggesting that hypoxia is a potent inducer of EHT in zebrafish. These data are consistent with a recent report showing that aortic ECs emerging from the DA in mice are hypoxic.[24]

The Hif-1α pathway has been suggested to regulate EHT on the basis of MO studies.[23,24] Recently, several publications have highlighted the phenotypic differences between morphants and mutants[56-58] and the importance of validating the morphant phenotypes described in the past.[59] Here, using *hif-1α* and *hif-2α* mutants, we confirm the previous MO studies on the role of *hif-1α* during EHT and describe a novel role for *hif-2α* in this process. Importantly, by using time-lapse imaging, we found that the reduction in HE cell number in the VDA is the likely cause of the HSC defects in *hif-1α*$^{-/-}$ and *hif-2α*$^{-/-}$, a novel observation. HIF-1α and HIF-2α have been described to have both distinct and overlapping roles, depending on the biological context.[42] A previous article has reported a partial loss of HSC

number in *Hif-1α*-mutant mice.[24] Here, we suggest that this observation may be due, at least in part, to HIF-2α, which may be able to compensate partially for the loss of HIF-1α.

HIF is mainly involved in the transcriptional activation of hypoxia-responsive genes, and recent studies have suggested that the HIF transcriptional complex may interact with certain signaling pathways, including Notch. Here, our data suggest that Hif and Notch function in the same pathway during EHT. Specifically, NICD overexpression in ECs could rescue the HSC defects observed in *hif-1α* and *hif-2α* mutants, suggesting that Notch functions downstream of Hif. Given the multiple roles of Notch signaling in developmental processes, it is possible that Notch could also be acting upstream or in parallel to Hif. The relationship between the Notch and Hif pathways is also context specific and has been explored in different settings; a recent article showed that in crystal cells (a blood cell type in *Drosophila*), *sima*, the ortholog of *Hif-1α*, activates Notch receptor in both normoxic and hypoxic cells in a cell-autonomous manner.[60]

Our study provides new insights into the role of hypoxia and the Hif pathway in definitive hematopoiesis, and our genetic analyses provide a link between the Hif pathway and Notch signaling. These data help further understand the players and microenvironment that modulate HSC formation, which will have an impact on the ways HE-derived HSCs are generated for therapeutic purposes.

Acknowledgments

The authors thank Michelle M. Collins, Anabela Bensimon-Brito, Jason Kuan Han Lai, Felix Gunawan, Hyouk-Bum Kwon, S. Javad Rasouli, Kenny Mattonet, Silvia Parajes Castro, and Ryota Matsuoka for sharing reagents and protocols; Francesca Luzzani for support in some experiments; members of the Stainier Laboratory, in particular Rubén Marín-Juez, for helpful discussions.

The Max Planck Society, International Max Planck Research Schools, Deutsche Forschungsgemeinschaft (SFB 834) provided funding.

Authorship

Contribution: C.G., M.M., and D.Y.R.S. designed experiments and analyzed data; C.G. and M.M. conducted experiments; A.R. contributed an unpublished reagent; and C.G., M.M., and D.Y.R.S. wrote the paper with feedback from all authors.

Conflict-of-interest disclosure: The authors declare no competing financial interests.

ORCID profile: C.G., 0000-0002-9046-3820.

Correspondence: Didier Y.R. Stainier, Max Planck Institute for Heart and Lung Research, Developmental Genetics (Dept. III), Ludwigstraße 43, 61231 Bad Nauheim, Germany; e-mail: didier.stainier@mpi-bn.mpg.de.

Footnotes

Submitted 21 July 2017; accepted 5 January 2018. Prepublished online as *Blood* First Edition paper, 16 January 2018; DOI 10.1182/blood-2017-07-797795.

*C.G. and M.M. contributed equally to this study.

The online version of this article contains a data supplement.

The publication costs of this article were defrayed in part by page charge payment. Therefore, and solely to indicate this fact, this article is hereby marked "advertisement" in accordance with 18 USC section 1734.

REFERENCES

1. Orkin SH, Zon LI. Hematopoiesis: an evolving paradigm for stem cell biology. *Cell*. 2008; 132(4):631-644.
2. Taoudi S, Medvinsky A. Functional identification of the hematopoietic stem cell niche in the ventral domain of the embryonic dorsal aorta. *Proc Natl Acad Sci USA*. 2007;104(22): 9399-9403.
3. Jaffredo T, Gautier R, Brajeul V, Dieterlen-Lièvre F. Tracing the progeny of the aortic hemangioblast in the avian embryo. *Dev Biol*. 2000;224(2):204-214.
4. Boisset JC, van Cappellen W, Andrieu-Soler C, Galjart N, Dzierzak E, Robin C. In vivo imaging of haematopoietic cells emerging from the mouse aortic endothelium. *Nature*. 2010; 464(7285):116-120.
5. Bertrand JY, Chi NC, Santoso B, Teng S, Stainier DY, Traver D. Haematopoietic stem cells derive directly from aortic endothelium during development. *Nature*. 2010;464(7285): 108-111.
6. Kissa K, Herbomel P. Blood stem cells emerge from aortic endothelium by a novel type of cell transition. *Nature*. 2010;464(7285): 112-115.
7. Chen MJ, Yokomizo T, Zeigler BM, Dzierzak E, Speck NA. Runx1 is required for the endothelial to haematopoietic cell transition but not thereafter. *Nature*. 2009;457(7231): 887-891.
8. North T, Gu TL, Stacy T, et al. Cbfa2 is required for the formation of intra-aortic hematopoietic clusters. *Development*. 1999; 126(11):2563-2575.
9. Kalev-Zylinska ML, Horsfield JA, Flores MV, et al. Runx1 is required for zebrafish blood and vessel development and expression of a human RUNX1-CBF2T1 transgene advances a model for studies of leukemogenesis. *Development*. 2002;129(8):2015-2030.
10. Wilkinson RN, Pouget C, Gering M, et al. Hedgehog and Bmp polarize hematopoietic stem cell emergence in the zebrafish dorsal aorta. *Dev Cell*. 2009;16(6):909-916.
11. Sood R, English MA, Belele CL, et al. Development of multilineage adult hematopoiesis in the zebrafish with a runx1 truncation mutation. *Blood*. 2010;115(14):2806-2809.
12. Kumano K, Chiba S, Kunisato A, et al. Notch1 but not Notch2 is essential for generating hematopoietic stem cells from endothelial cells. *Immunity*. 2003;18(5):699-711.
13. Butko E, Distel M, Pouget C, et al. Gata2b is a restricted early regulator of hemogenic endothelium in the zebrafish embryo. *Development*. 2015;142(6):1050-1061.
14. Robert-Moreno A, Espinosa L, de la Pompa JL, Bigas A. RBPjkappa-dependent Notch function regulates Gata2 and is essential for the formation of intra-embryonic hematopoietic cells. *Development*. 2005;132(5): 1117-1126.
15. Gao X, Johnson KD, Chang YI, et al. Gata2 cis-element is required for hematopoietic stem cell generation in the mammalian embryo. *J Exp Med*. 2013;210(13):2833-2842.
16. Hadland BK, Huppert SS, Kanungo J, et al. A requirement for Notch1 distinguishes 2 phases of definitive hematopoiesis during development. *Blood*. 2004;104(10): 3097-3105.
17. Tsai FY, Keller G, Kuo FC, et al. An early haematopoietic defect in mice lacking the transcription factor GATA-2. *Nature*. 1994; 371(6494):221-226.
18. Mucenski ML, McLain K, Kier AB, et al. A functional c-myb gene is required for normal murine fetal hepatic hematopoiesis. *Cell*. 1991;65(4):677-689.
19. Thomas MD, Kremer CS, Ravichandran KS, Rajewsky K, Bender TP. c-Myb is critical for B cell development and maintenance of follicular B cells. *Immunity*. 2005;23(3):275-286.
20. Sandberg ML, Sutton SE, Pletcher MT, et al. c-Myb and p300 regulate hematopoietic stem cell proliferation and differentiation. *Dev Cell*. 2005;8(2):153-166.

21. Badiani P, Corbella P, Kioussis D, Marvel J, Weston K. Dominant interfering alleles define a role for c-Myb in T-cell development. *Genes Dev*. 1994;8(7):770-782.

22. Zhang Y, Jin H, Li L, Qin FX, Wen Z. cMyb regulates hematopoietic stem/progenitor cell mobilization during zebrafish hematopoiesis. *Blood*. 2011;118(15):4093-4101.

23. Harris JM, Esain V, Frechette GM, et al. Glucose metabolism impacts the spatiotemporal onset and magnitude of HSC induction in vivo. *Blood*. 2013;121(13):2483-2493.

24. Imanirad P, Solaimani Kartalaei P, Crisan M, et al. HIF1α is a regulator of hematopoietic progenitor and stem cell development in hypoxic sites of the mouse embryo. *Stem Cell Res (Amst)*. 2014;12(1):24-35.

25. Westerfield M. The Zebrafish Book: A Guide for the Laboratory Use of Zebrafish (Danio rerio). 4th ed. Eugene, OR: University of Oregon Press; 2000.

26. Chi NC, Shaw RM, De Val S, et al. Foxn4 directly regulates tbx2b expression and atrioventricular canal formation. *Genes Dev*. 2008; 22(6):734-739.

27. Jin SW, Beis D, Mitchell T, Chen JN, Stainier DY. Cellular and molecular analyses of vascular tube and lumen formation in zebrafish. *Development*. 2005;132(23):5199-5209.

28. North TE, Goessling W, Walkley CR, et al. Prostaglandin E2 regulates vertebrate haematopoietic stem cell homeostasis. *Nature*. 2007;447(7147):1007-1011.

29. Scheer N, Groth A, Hans S, Campos-Ortega JA. An instructive function for Notch in promoting gliogenesis in the zebrafish retina. *Development*. 2001;128(7):1099-1107.

30. Scheer N, Campos-Ortega JA. Use of the Gal4-UAS technique for targeted gene expression in the zebrafish. *Mech Dev*. 1999; 80(2):153-158.

31. Herwig L, Blum Y, Krudewig A, et al. Distinct cellular mechanisms of blood vessel fusion in the zebrafish embryo. *Curr Biol*. 2011;21(22): 1942-1948.

32. Jao LE, Wente SR, Chen W. Efficient multiplex biallelic zebrafish genome editing using a CRISPR nuclease system. *Proc Natl Acad Sci USA*. 2013;110(34):13904-13909.

33. Gerri C, Marín-Juez R, Marass M, Marks A, Maischein HM, Stainier DY. Hif-1α regulates macrophage-endothelial interactions during blood vessel development in zebrafish. *Nat Commun*. 2017;8:15492.

34. Cermak T, Doyle EL, Christian M, et al. Efficient design and assembly of custom TALEN and other TAL effector-based constructs for DNA targeting. *Nucleic Acids Res*. 2011;39(12):e82.

35. Dahlem TJ, Hoshijima K, Jurynec MJ, et al. Simple methods for generating and detecting locus-specific mutations induced with TALENs in the zebrafish genome. *PLoS Genet*. 2012; 8(8):e1002861.

36. Peterson SM, Freeman JL. RNA isolation from embryonic zebrafish and cDNA synthesis for gene expression analysis. *J Vis Exp*. 2009; (30).

37. Thisse C, Thisse B. High-resolution in situ hybridization to whole-mount zebrafish embryos. *Nat Protoc*. 2008;3(1):59-69.

38. Metelo AM, Noonan HR, Li X, et al. Pharmacological HIF2α inhibition improves VHL disease-associated phenotypes in zebrafish model. *J Clin Invest*. 2015;125(5): 1987-1997.

39. Mendelsohn BA, Kassebaum BL, Gitlin JD. The zebrafish embryo as a dynamic model of anoxia tolerance. *Dev Dyn*. 2008;237(7): 1780-1788.

40. Hwang WY, Fu Y, Reyon D, et al. Efficient genome editing in zebrafish using a CRISPR-Cas system. *Nat Biotechnol*. 2013;31(3): 227-229.

41. Zhen F, Lan Y, Yan B, Zhang W, Wen Z. Hemogenic endothelium specification and hematopoietic stem cell maintenance employ distinct Scl isoforms. *Development*. 2013; 140(19):3977-3985.

42. Keith B, Johnson RS, Simon MC. HIF1α and HIF2α: sibling rivalry in hypoxic tumour growth and progression. *Nat Rev Cancer*. 2011;12(1):9-22.

43. Nottingham WT, Jarratt A, Burgess M, et al. Runx1-mediated hematopoietic stem-cell emergence is controlled by a Gata/Ets/SCL-regulated enhancer. *Blood*. 2007;110(13): 4188-4197.

44. Busch-Nentwich E, Kettleborough R, Dooley CM, et al. Sanger Institute Zebrafish Mutation Project mutant data submission. *ZFIN Direct Data Submission*. 2013. http://zfin.org.

45. Burns CE, Traver D, Mayhall E, Shepard JL, Zon LI. Hematopoietic stem cell fate is established by the Notch-Runx pathway. *Genes Dev*. 2005;19(19):2331-2342.

46. Konantz M, Alghisi E, Müller JS, et al. Evi1 regulates Notch activation to induce zebrafish hematopoietic stem cell emergence. *EMBO J*. 2016;35(21):2315-2331.

47. Riddell J, Gazit R, Garrison BS, et al. Reprogramming committed murine blood cells to induced hematopoietic stem cells with defined factors. *Cell*. 2014;157(3):549-564.

48. Sandler VM, Lis R, Liu Y, et al. Reprogramming human endothelial cells to haematopoietic cells requires vascular induction. *Nature*. 2014;511(7509):312-318.

49. Doulatov S, Vo LT, Chou SS, et al. Induction of multipotential hematopoietic progenitors from human pluripotent stem cells via respecification of lineage-restricted precursors. *Cell Stem Cell*. 2013;13(4):459-470.

50. Pereira C-F, Chang B, Qiu J, et al. Induction of a hemogenic program in mouse fibroblasts. *Cell Stem Cell*. 2013;13(2):205-218.

51. Szabo E, Rampalli S, Risueño RM, et al. Direct conversion of human fibroblasts to multilineage blood progenitors. *Nature*. 2010; 468(7323):521-526.

52. Batta K, Florkowska M, Kouskoff V, Lacaud G. Direct reprogramming of murine fibroblasts to hematopoietic progenitor cells. *Cell Reports*. 2014;9(5):1871-1884.

53. Sugimura R, Jha DK, Han A, et al. Haematopoietic stem and progenitor cells from human pluripotent stem cells. *Nature*. 2017;545(7655):432-438.

54. Lis R, Karrasch CC, Poulos MG, et al. Conversion of adult endothelium to immunocompetent haematopoietic stem cells. *Nature*. 2017;545(7655):439-445.

55. Elks PM, Renshaw SA, Meijer AH, Walmsley SR, van Eeden FJ. Exploring the HIFs, buts and maybes of hypoxia signalling in disease: lessons from zebrafish models. *Dis Model Mech*. 2015;8(11):1349-1360.

56. Kok FO, Shin M, Ni CW, et al. Reverse genetic screening reveals poor correlation between morpholino-induced and mutant phenotypes in zebrafish. *Dev Cell*. 2015;32(1):97-108.

57. Place ES, Smith JC. Zebrafish atoh8 mutants do not recapitulate morpholino phenotypes. *PLoS One*. 2017;12(2):e0171143.

58. Rossi A, Kontarakis Z, Gerri C, et al. Genetic compensation induced by deleterious mutations but not gene knockdowns. *Nature*. 2015; 524(7564):230-233.

59. Stainier DYR, Raz E, Lawson ND, et al. Guidelines for morpholino use in zebrafish. *PLoS Genet*. 2017;13(10):e1007000.

60. Mukherjee T, Kim WS, Mandal L, Banerjee U. Interaction between Notch and Hif-α in development and survival of Drosophila blood cells. *Science*. 2011;332(6034): 1210-1213.